Cloaking through cancellation of diffusive wave scattering

Mohamed Farhat, Pai-Yen Chen, Sébastien Guenneau, Hakan Bagci, Khaled Nabil Salama, Andrea Alu

Cloaking through cancellation of diffusive wave scattering

M. Farhat[1], P. Y. Chen[2], S. Guenneau[3], H. Bağcı[1], K. N. Salama[1] and A. Alù[4]

[1]Division of Computer, Electrical, and Mathematical Sciences and Engineering, King Abdullah University of Science and Technology (KAUST), Thuwal 23955-6900, Saudi Arabia
[2]Department of Electrical and Computer Engineering, Wayne State University, Detroit, MI 48202, USA
[3]Aix-Marseille Université, CNRS, Centrale Marseille, Institut Fresnel, Campus universitaire de Saint-Jérôme, 13013 Marseille, France
[4]Department of Electrical and Computer Engineering, The University of Texas at Austin, Austin, TX 78712, USA

A new cloaking mechanism, which makes enclosed objects invisible to diffusive photon density waves, is proposed. First, diffusive scattering from a basic core–shell geometry, which represents the cloaked structure, is studied. The conditions of scattering cancellation in a quasi-static scattering regime are derived. These allow for tailoring the diffusivity constant of the shell enclosing the object so that the fields scattered from the shell and the object cancel each other. This means that the photon flow outside the cloak behaves as if the cloaked object were not present. Diffusive light invisibility may have potential applications in hiding hot spots in infrared thermography or tissue imaging.

1. Introduction

Invisibility cloaks, which were first introduced 10 years ago [1–4], are still one of the most interesting and popular applications of metamaterials [5]. They have applications in various fields of engineering, such as sensing [6] and imaging [7]. In the past few years, numerous methods were suggested to make objects invisible to electromagnetic radiation [8,9]. The first attempt can be traced back to coated ellipsoidal and spherical dielectric scatterers proposed by Kerker [10,11]. He showed that, in

the static regime, some combinations of the permittivities of the coating shell and the core lead to cancellation of the fields scattered from the whole structure. Alù and Engheta further investigated the scattering cancellation technique (SCT) and showed that using a carefully designed plasmonic shell also leads to invisibility [12–14]. This technique is robust since it makes use of homogeneous layers [14], and its applicability was demonstrated by experiments [15]. Variants of the scattering cancellation technique were also investigated; these include constructing an effective coating using plasmonic nanoparticles [16,17] and mantle (ultra-thin) covers [18,19]. Additionally, other methods making use of homogenization techniques were shown to generate broadband cloaking against electromagnetic [20,21] or acoustic [22] radiation.

The scattering cancellation technique, which was originally developed for cloaking scatterers under electromagnetic excitation, as briefly described above, was successfully adapted to make objects invisible to other types of waves. Chen and co-workers [23,24] and Guild *et al.* [25,26] showed, quite simultaneously, that a spherical object could be made invisible to acoustic pressure waves by coating it with an ultra-thin shell of carefully tailored acoustic impedance. Additionally, the same technique was shown to have potential in designing invisibility cloaks for elastic [27] and thermal [28] waves.

In this work, the scattering cancellation technique is used to design cloaks for objects under excitation by diffusive photon density waves (DPDWs), i.e. light waves propagating in a turbid medium such as biological tissue and dusty/foggy air [29]. The photons propagating in such a medium experience the multiple scattering phenomenon [30]. Even though, the individual photons follow random paths, macroscopically, they behave as a density wave that is described by a Helmholtz-like partial differential equation and experience regular wave phenomena such as refraction [31] and scattering [30]. Unsurprisingly, cloaks making use of transformation optics were designed to make objects in turbid media invisible to such kind of waves [32,33]. Along the same lines, a cloak making use of the scattering cancellation technique is proposed here, for a more general diffusion equation (DPDW). To this end, first, the scattering of DPDWs from core–shell structures is studied, then the conditions of scattering cancellation in a quasi-static regime are derived. There, cloaks have promising applications in medical tissue imaging [34,35] and heat-assisted magnetic recording (HAMR-technology) [36].

2. Dispersion relation and Helmholtz-like equation for diffusive photon density waves

Using the first principle of thermodynamics in a closed system and in the absence of radiation and convection, one can show that the photon number density of a DPDW, Φ, obeys the relation $\nabla \cdot \mathbf{j} + \partial \Phi / \partial t + \upsilon \mu_a \Phi + \upsilon \varsigma = 0$. Here, $\mathbf{j}$, υ, μ_a and ς represent the photon current density (photon flow per unit surface and per unit time), the speed of light in the diffusive medium, the absorption coefficient and the source of photons, respectively. Using Fick's first law, i.e. the relation $\mathbf{j} = -D\nabla \Phi$, one can derive

$$\frac{\partial \Phi(\mathbf{r}, t)}{\partial t} + \upsilon \mu_a \Phi(\mathbf{r}, t) + \upsilon \varsigma(\mathbf{r}_s, t) = \nabla \cdot [D\nabla \Phi(\mathbf{r}, t)]. \tag{2.1}$$

The diffusivity $D = \upsilon/[3(\mu_a + \mu_s)]$ and it simplifies to $\upsilon/(3\mu_s)$ under the P_1 approximation, i.e. $\mu_a \ll \mu_s$ [37–39], where μ_s is the scattering coefficient in the medium. Assuming a piecewise constant D and a time harmonic excitation (i.e. $e^{-i\omega t}$ dependence) equation (2.1) becomes

$$\Delta \Phi(r) + \left(\frac{i\omega - \upsilon \mu_a}{D}\right) \Phi(r) = \upsilon \varsigma(r). \tag{2.2}$$

The above equation shows that Φ satisfies a Helmholtz-like equation $\Delta \Phi + \kappa^2 \Phi = 0$, with a complex wavenumber κ related to the frequency through the dispersion relation $\kappa^2 = (i\omega - \upsilon \mu_a)/D$. Inserting the parameters of water, i.e. a diffusivity $D_0 = 1.75 \times 10^6 \, \mathrm{m^2 \, s^{-1}}$ and lifetime of the photons $1/(\upsilon_0 \mu_{a,0}) = 30 \times 10^{-9} \, \mathrm{s}$ into this dispersion relation, one obtains the plot shown in figure 1b. Note that here the subscript 0 denotes the properties of the background medium where
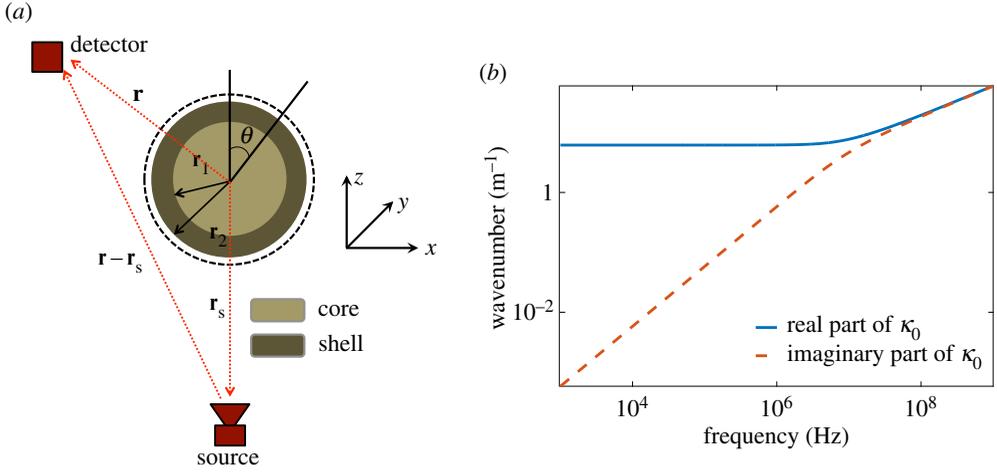
Figure 1. (*a*) Cross section of the core–shell structure used for studying the scattering of DPDWs. (*b*) Dispersion relation in the background medium, region 0: Real and imaginary parts of κ_0 versus frequency. (Online version in colour.)

the cloak is residing. In particular, one can notice that the real part of κ_0 tends asymptotically to the limit $\sqrt{\upsilon_0\mu_{a,0}/D_0}$ when the frequency goes to zero, and is much higher than its imaginary part, due to absorption. At higher frequencies ($\omega \gg \upsilon_0\mu_{a,0}$), the real and imaginary parts are equal (since κ_0^2 is purely imaginary, as can be seen in figure 1*b*).

3. Analysis of diffusive photon density wave scattering

In this section, to study the scattering of DPDWs, it is assumed that they are generated by a sinusoidally modulated point source in the turbid background medium (region 0) [31,40]. The resulting DPDWs are spherical waves that propagate outwards from the point source, and it is assumed that they are incident on a spherical core–shell structure, as schematized in figure 1*a*. The object is coated with a cloaking shell made of a material with tailored parameters. Parameters of object and cloak materials are identified using subscripts 1 and 2, respectively. It can be shown that Φ can be found by constructing general solutions of equation (2.2) in regions 0, 1, and 2 as shown in figure 1*a* and applying the proper boundary conditions. Without loss of generality, it is assumed that the origin of the spherical coordinates coincides with the centre of the core–shell structure (figure 1*a*).

(a) Scattering of spherical objects

For the solutions constructed in this section, it is assumed that D_1 and $\upsilon_1\mu_{a,1}$ have finite values. In region 0, the general solution is the superposition of incident and scattered waves, i.e. $\Phi^0 = \Phi^{\text{inc}} + \Phi^{\text{scat}}$, where

$$\Phi^{\text{inc}}(r,\theta,\varphi) = \frac{\upsilon\varsigma}{4\pi D_0|\mathbf{r}-\mathbf{r}_s|}\,e^{i\kappa_0|\mathbf{r}-\mathbf{r}_s|}$$

$$= i\frac{\upsilon\varsigma\kappa_0}{D_0}\sum_{l=0}^{\infty}j_l(\kappa_0 r_<)h_l^{(1)}(\kappa_0 r_>)\sum_{m=-l}^{l}Y_{l,m}^*(\theta_s,\varphi_s)Y_{l,m}(\theta,\varphi), \quad (3.1)$$

is the spherical wave created by the source as shown in figure 1*a*, $\mathbf{r}_s$ is the position of the source, and $r_<$ and $r_>$ denote the smaller and larger of $|\mathbf{r}|$ and $|\mathbf{r}_s|$, respectively. In equation (3.1), * represents the complex conjugate. The wave scattered from the structure can be expressed as

$$\Phi^{\text{scat}}(r,\theta,\varphi) = \sum_{l,m}s_{l,m}h_l^{(1)}(\kappa_0 r)Y_{l,m}(\theta,\varphi), \quad r > r_2. \quad (3.2)$$

In region 1, the solution is

$$\Phi^1(r,\theta,\varphi) = \sum_{l,m} a_{l,m} j_l(\kappa_1 r) Y_{l,m}(\theta,\varphi), \quad r < r_1. \tag{3.3}$$

In region 2, the solution is

$$\Phi^2(r,\theta,\varphi) = \sum_{l,m} [b_{l,m} j_l(\kappa_2 r) + c_{l,m} y_l(\kappa_2 r)] Y_{l,m}(\theta,\varphi), \quad r_1 < r \le r_2. \tag{3.4}$$

Here, j_l and y_l, and $h_l^{(1)}$ are spherical Bessel functions of the first and the second kinds, and the Hankel function of the first kind, respectively, and $Y_{l,m}$ are the spherical harmonics and κ_0, κ_1, and κ_2 denote the complex wavenumbers in regions 0, 1, and 2, respectively. The coefficients $a_{l,m}$, $b_{l,m}$, $c_{l,m}$, and $s_{l,m}$ can be determined using the following conditions: (i) Φ is finite for $\mathbf{r} \ne \mathbf{r}_s$. (ii) When $r \to \infty$, Φ^0 tends asymptotically to a spherically outgoing wave. (iii) The normal component of the flux is continuous on the surfaces between the different regions, i.e. $D_1 \partial \Phi^1/\partial r = D_2 \partial \Phi^2/\partial r$ at $r = r_1$ and $D_2 \partial \Phi^2/\partial r = D_0 \partial \Phi^0/\partial r$ at $r = r_2$. (iv) Φ is continuous on the surfaces between the different regions, i.e. $\Phi^1(r_1) = \Phi^2(r_1)$ and $\Phi^2(r_2) = \Phi^0(r_2)$.

To simplify the calculations, without loss of generality, it is assumed that the source is located on the z-axis (i.e. $\theta_s = \pi$) and $\varphi_s = 0$. This means that the terms with $m \ne 0$ are zero. Using the conditions (i)–(iv) above together with the solutions in equations (3.1)–(3.4) under this assumption, one can find the scattered field coefficients as $s_l = -\psi_l/(\psi_l + i\chi_l)$. Here, ψ_l and χ_l are given by the complex-valued determinants

$$\psi_l = \begin{vmatrix} -j_l(\kappa_1 r_1) & y_l(\kappa_2 r_1) & j_l(\kappa_2 r_1) & 0 \\ -D_1\kappa_1 j_l'(\kappa_1 r_1) & D_2\kappa_2 y_l'(\kappa_2 r_1) & D_2\kappa_2 j_l'(\kappa_2 r_1) & 0 \\ 0 & y_l(\kappa_2 r_2) & j_l(\kappa_2 r_2) & \alpha_l j_l(\kappa_0 r_2) \\ 0 & D_2\kappa_2 y_l'(\kappa_2 r_2) & D_2\kappa_2 j_l'(\kappa_2 r_2) & D_0\kappa_0 \alpha_l j_l'(\kappa_0 r_2) \end{vmatrix} \tag{3.5}$$

and

$$\chi_l = \begin{vmatrix} -j_l(\kappa_1 r_1) & y_l(\kappa_2 r_1) & j_l(\kappa_2 r_1) & 0 \\ -D_1\kappa_1 j_l'(\kappa_1 r_1) & D_2\kappa_2 y_l'(\kappa_2 r_1) & D_2\kappa_2 j_l'(\kappa_2 r_1) & 0 \\ 0 & y_l(\kappa_2 r_2) & j_l(\kappa_2 r_2) & \alpha_l y_l(\kappa_0 r_2) \\ 0 & D_2\kappa_2 y_l'(\kappa_2 r_2) & D_2\kappa_2 j_l'(\kappa_2 r_2) & D_0\kappa_0 \alpha_l y_l'(\kappa_0 r_2) \end{vmatrix}, \tag{3.6}$$

where $\alpha_l = i(\upsilon \varsigma \kappa_0/D_0) j_l(\kappa_0 |\mathbf{r}_s|) Y_{l,m}^*(\pi, 0)$.

The scattering cross section (SCS), σ^{scat}, is a measure of the overall visibility of the object to external observers. It is obtained by integrating the scattering amplitude, defined as $g(\theta,\varphi) \approx r\,e^{-i\kappa_0 r} \Phi^{\text{scat}}/|\Phi^{\text{inc}}|$ when $r \to \infty$, over the full solid angle [24]

$$\sigma^{\text{scat}} = \frac{4\pi}{|\kappa_0|^2} \sum_{l=0}^{\infty} (2l+1) \frac{|\psi_l|^2}{|\psi_l + i\chi_l|^2}. \tag{3.7}$$

In the quasi-static limit (long diffusion length $\kappa_i r_j \ll 1$, where $(i,j) \subset (0,1,2)$), only the first few terms in the summation in equation (3.7) contribute to the SCS. Here, it is assumed that the first two terms ($l=0$ for the monopole and $l=1$ for the dipole mode, unlike in the electromagnetic case, where the first dominant mode is the dipole mode) are significant. Under this assumption, one has $\sigma^{\text{scat}} \approx 4\pi/|\kappa_0|^2(|s_0|^2 + 3|s_1|^2)$. Consequently, cancelling these two modes, i.e. $s_0 = 0$ ($\psi_0 = 0$ and $\chi_0 \ne 0$) and $s_1 = 0$ ($\psi_1 = 0$ and $\chi_1 \ne 0$) ensures that $\sigma^{\text{scat}} \approx 0$, and the *diffusive* scattering from

the object is suppressed. These conditions, which are termed here as the SCT conditions, yield the parameters of the cloaking shell D_2, $\upsilon_2\mu_{a,2}$ and r_2 as

$$\frac{(1 + i\upsilon_2\mu_{a,2}/\omega) - (1 + i\upsilon_0\mu_{a,0}/\omega)}{(1 + i\upsilon_2\mu_{a,2}/\omega) - (1 + i\upsilon_1\mu_{a,1}/\omega)} = \frac{\upsilon_2\mu_{a,2} - \upsilon_0\mu_{a,0}}{\upsilon_2\mu_{a,2} - \upsilon_1\mu_{a,1}} = \gamma^3, \quad \text{for } \psi_0 = 0 \tag{3.8}$$

and

$$\frac{(D_0 - D_2)(D_1 + 2D_2)}{(D_1 - D_2)(D_0 + 2D_2)} = \gamma^3, \quad \text{for } \psi_1 = 0, \tag{3.9}$$

where $\gamma = r_1/r_2$. The conditions in equations (3.8) and (3.9) are used to obtain the material properties of the shell and γ in terms of the material properties of the object and background medium, for effective cloaking in the quasi-static regime.

(b) Perfectly absorbing spherical objects

In this section, conditions on the parameters of the shell material when region 1 is completely filled with a perfectly absorbing object are derived. The expressions of Φ^0 and Φ^2 given by equations (3.1), (3.2), and (3.4) remain unchanged but $\Phi^1 = 0$. Additionally, the boundary conditions at $r = r_2$ are the same as those used in the previous section, but at $r = r_1$, a zero partial flux boundary condition is enforced [30,35], i.e.

$$\frac{D_2}{2\upsilon_2} \frac{\partial \Phi^2(r,\theta,\varphi)}{\partial r}\bigg|_{r=r_1} - \frac{1}{4}\Phi^2(r_1,\theta,\varphi) = 0. \tag{3.10}$$

These new boundary conditions lead to the following expressions for ψ_l and χ_l:

$$\psi_l = \begin{vmatrix} \frac{D_2\kappa_2}{2\upsilon_2}y_l'(\kappa_2 r_1) - \frac{1}{4}y_l(\kappa_2 r_1) & \frac{D_2\kappa_2}{2\upsilon_2}j_l'(\kappa_2 r_1) - \frac{1}{4}j_l(\kappa_2 r_1) & 0 \\ y_l(\kappa_2 r_2) & j_l(\kappa_2 r_2) & \alpha_l j_l(\kappa_0 r_2) \\ D_2\kappa_2 y_l'(\kappa_2 r_2) & D_2\kappa_2 j_l'(\kappa_2 r_2) & D_0\kappa_0\alpha_l j_l'(\kappa_0 r_2) \end{vmatrix} \tag{3.11}$$

and

$$\chi_l = \begin{vmatrix} \frac{D_2\kappa_2}{2\upsilon_2}y_l'(\kappa_2 r_1) - \frac{1}{4}y_l(\kappa_2 r_1) & \frac{D_2\kappa_2}{2\upsilon_2}j_l'(\kappa_2 r_1) - \frac{1}{4}j_l(\kappa_2 r_1) & 0 \\ y_l(\kappa_2 r_2) & j_l(\kappa_2 r_2) & \alpha_l y_l(\kappa_0 r_2) \\ D_2\kappa_2 y_l'(\kappa_2 r_2) & D_2\kappa_2 j_l'(\kappa_2 r_2) & D_0\kappa_0\alpha_l y_l'(\kappa_0 r_2) \end{vmatrix}. \tag{3.12}$$

In the quasi-static limit, for $l = 0$, one has

$$\psi_0 \approx \frac{D_2\kappa_2}{4\kappa_2^2 r_2^2}. \tag{3.13}$$

This means that, to cancel s_0, one should select $D_2 = 0$. It can be shown, after some straightforward algebra, that the condition which ensures that $s_1 = 0$ ($\psi_1 = 0$) is given by

$$\frac{D_2 - D_0}{2D_2 + D_0} = \frac{\gamma^3}{2}. \tag{3.14}$$

(c) Ultra-thin invisibility shells: mantle cloaking

The set-up of the scattering problem is the same as the ones described in the previous sections, except that the scattering reduction is achieved here by a three-dimensional metasurface introduced at $r = r_2$ instead of a thick shell. By tailoring the values of the metasurface's impedance, one can drastically reduce the scattering from the object it encloses. The boundary conditions at $r = r_1$ are the same as those described in §3a (continuity of Φ and $D_i\partial\Phi^i/\partial r$).

The boundary conditions at $r = r_2$ are $\Phi(r = r_2^-) = \Phi(r = r_2^+) = \Phi(r = r_2)$ and

$$\left.\frac{1}{\mu_{s,0}}\frac{\partial\Phi}{\partial n}\right|_{r=r_2^+} - \left.\frac{1}{\mu_{s,2}}\frac{\partial\Phi}{\partial n}\right|_{r=r_2^-} = \frac{3Z_d^{-1}}{v_0}\Phi(r_2),\tag{3.15}$$

where $Z_d = R_d + iX_d$ is the averaged surface impedance that relates the averaged fluence on the surface to its averaged flux. This impedance is a function of the geometry of the structure and the wavelength of the excitation and usually varies in a large range of values. Generally, Z_d is a complex-valued impedance (R_d and X_d are, respectively, related to resistive and reactive parts). Here, a lossless metasurface is assumed, and the metasurface is actually a reactance. Considering the effect of loss, will not sensibly affect the cloaking [18].

Using these boundary conditions together with the general solutions in equations (3.1)–(3.4), one can show that $s_l = 0$ provided that

$$\psi_l = \begin{vmatrix} -j_l(\kappa_1 r_1) & y_l(\kappa_0 r_1) & j_l(\kappa_0 r_1) & 0 \\ -D_1\kappa_1 j'_l(\kappa_1 r_1) & D_2\kappa_0 y'_l(\kappa_0 r_1) & D_2\kappa_0 j'_l(\kappa_0 r_1) & 0 \\ 0 & y_l(\kappa_0 r_2) & j_l(\kappa_0 r_2) & \alpha_l j_l(\kappa_0 r_2) \\ 0 & y'_l(\kappa_0 r_2) + \eta y_l(\kappa_0 r_2) & j'_l(\kappa_0 r_2) + \eta j_l(\kappa_0 r_2) & j'_l(\kappa_0 r_2) \end{vmatrix} = 0.\tag{3.16}$$

Here $\eta = i\omega/(Z_d D_0 \kappa_0 \alpha_l)$ is a dimensionless function. Solving the condition $\psi_0 = 0$ in the quasi-static limit yields

$$X_d = \frac{2v}{9\gamma^3\omega r_1}\left(\frac{\gamma^3}{\mu_{s,0}} + \frac{\mu_{s,1} + 2\mu_{s,0}}{\mu_{s,0}(\mu_{s,0} - \mu_{s,1})}\right).\tag{3.17}$$

This clearly demonstrates that by carefully choosing X_d, it is possible to suppress the dominant scattering term in the quasi-static regime.

4. Numerical modelling

(a) Ideal cloaking parameters

Equations (3.8) and (3.9) can be solved numerically to obtain the relation between different parameters of the core–shell structure, for the normalized wavenumber in background $\kappa_0 r_1 = 0.5$. Figure 2a plots $\mu_{a,2}$ versus $\mu_{a,1}$ and γ; the relation described by equation (3.8) when $\mu_{a,0} = 0.023\,\text{cm}^{-1}$, $\mu_{s,0} = 6\,\text{cm}^{-1}$, and $v_0 = v_1 = v_2$. One can see from this figure that $\mu_{a,2}$ takes positive and negative values, depending on γ and $\mu_{a,1}$. The thick line represents the curve obeying the equation $\gamma^3\mu_{a,1}/\mu_{a,0} = 1$, which means that $\mu_{a,2} = 0$. $\mu_{a,2}$ thus takes negative and positive near zero values above and below this curve, respectively. Similarly, figure 2b,c plot $\mu_{s,2}$ versus $\mu_{s,1}$ and γ; the relations described by the positive and negative solutions of equation (3.9) for the same parameters as before, respectively. On the other hand, for a small perfectly absorbing object, $\mu_{s,2}$ depends only on γ and is always positive, varying from $\mu_{s,0}$ to values close to zero as shown by figure 2d that plots the solution of equation (3.14).

(b) Cancelling scattering cross section

Two particular scenarios, where scattering of DPDWs from spherical objects is analysed, are considered in this section: (i) a scattering object with $\mu_{s,1} = 15\,\text{cm}^{-1}$ and $\mu_{a,1} = \mu_{a,0}$ and (ii) an absorbing object with $\mu_{s,1} = \mu_{s,0}$ and $\mu_{a,1} = 0.15\,\text{cm}^{-1}$. In both scenarios, $\mu_{s,0} = 6\,\text{cm}^{-1}$, $\mu_{a,0} = 0.023\,\text{cm}^{-1}$ in the background turbid medium (the P_1 approximation is valid). These values correspond to realistic materials [30]. The radii of both objects are $r_1 = 1.2\,\text{cm}$. These two objects are then coated with a shell of radius $r_2 = 1.35\,\text{cm}$. In both scenarios, the SCS of the total structure σ_2^{scat} is computed using equation (3.7), and normalized with the SCS of the bare (uncloaked) objects σ_1^{scat}. The results are plotted (in logarithmic scale) in figure 3a,b for scenarios (i) and (ii), respectively. While varying $\mu_{s,2}$ and $\mu_{a,2}$, it can be observed that there are dark and white regions
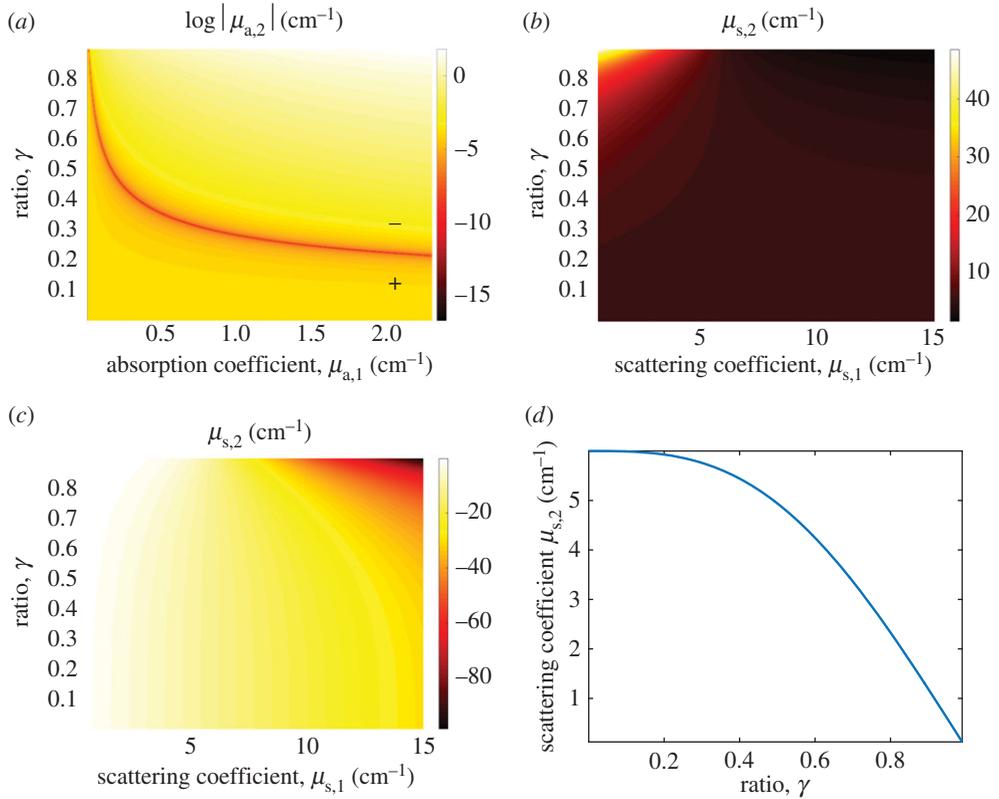
Figure 2. (a) Optimal absorption coefficient $\mu_{a,2}$ versus $\mu_{a,1}$ and γ. (b) Positive and (c) negative solutions of equation (3.9) giving contours of $\mu_{s,1}$ and γ. (d) $\mu_{s,2}$ given by equation (3.14) for a perfectly absorbing object. (Online version in colour.)
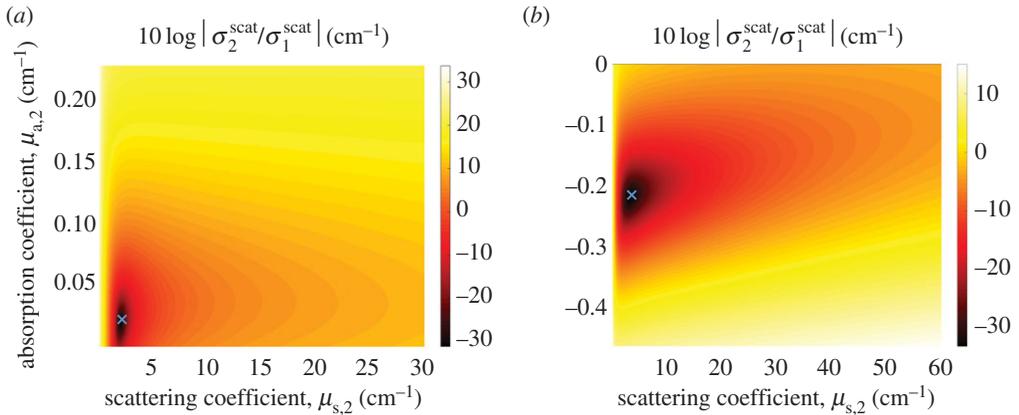

Figure 3. The SCS of the total structure σ_2^{scat} normalized with the SCS of the bare object σ_1^{scat} versus $\mu_{s,2}$ and $\mu_{a,2}$ for (a) a 'scattering' object with $\mu_{s,1} = 2.5\mu_{s,0} = 15\,\mathrm{cm}^{-1}$ and $\mu_{a,1} = \mu_{a,0} = 0.023\,\mathrm{cm}^{-1}$ and (b) an 'absorbing' object with $\mu_{s,1} = \mu_{s,0} = 6\,\mathrm{cm}^{-1}$ and $\mu_{a,1} = 6.5\mu_{a,0} = 0.15\,\mathrm{cm}^{-1}$. The crosses represent the positions of optimized scattering reduction, with a value of -35 dB. (Online version in colour.)

corresponding to a very large scattering reduction and increased scattering from the structure, respectively. For the scattering object (figure 3a), values of $\mu_{s,2}$ between 1.5 and 3.75 cm^{-1} and $\mu_{a,2}$ between 0.01 and 0.045 cm^{-1} are ideal for DPDWs scattering cancellation (black spot). In particular, the minimum of σ^{scat} is obtained for $\mu_{s,2} = 2.1\,\mathrm{cm}^{-1}$ and $\mu_{a,2} = 0.028\,\mathrm{cm}^{-1}$, which
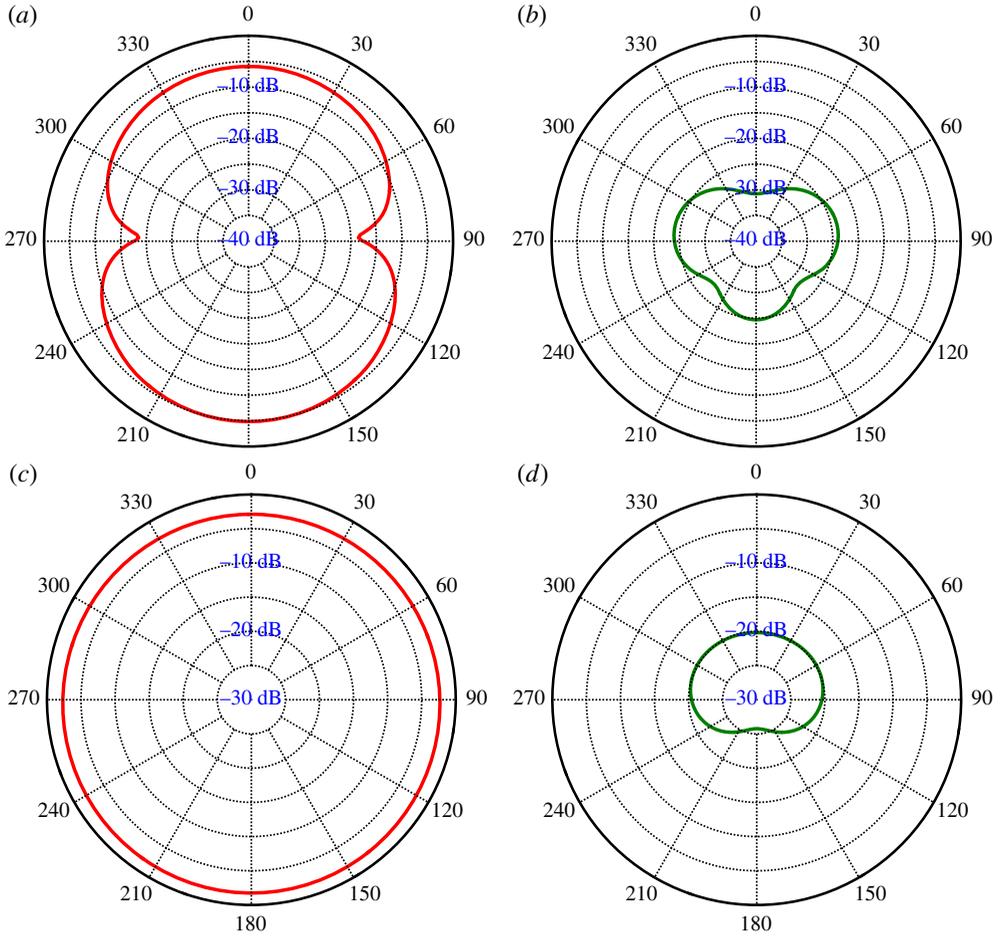
Figure 4. Far-field scattering amplitudes in polar coordinates, (*a*) for the bare scattering object with $\mu_{s,1} = 15\,\text{cm}^{-1}$ and $\mu_{a,1} = 0.023\,\text{cm}^{-1}$, (*b*) for the cloaked scattering object with $\mu_{s,2} = 2.1\,\text{cm}^{-1}$ and $\mu_{a,2} = 0.028\,\text{cm}^{-1}$, (*c*) for the bare absorbing object with $\mu_{s,1} = 6\,\text{cm}^{-1}$ and $\mu_{a,1} = 0.15\,\text{cm}^{-1}$ and (*d*) for the cloaked absorbing object with $\mu_{s,2} = 7\,\text{cm}^{-1}$ and $\mu_{a,2} = -0.25\,\text{cm}^{-1}$. (Online version in colour.)

fits very well with the predictions of equations (3.8), and (3.9), given by the crosses. For the absorbing object (figure 3*b*), values of $\mu_{s,2}$ between 1 and 15 cm^{-1} and $\mu_{a,2}$ between -0.15 and -0.28 cm^{-1} are ideal for DPDWs scattering cancellation (black spot). In particular, the minimum of σ^{scat} is obtained for $\mu_{s,2} = 7$ cm^{-1} and $\mu_{a,2} = -0.25$ cm^{-1}, which fits as well with the predictions of equations (3.8), and (3.9), given by the cross. By comparing figure 3*a,b*, one can also notice that in the first case, sensitivity to $\mu_{s,2}$ is more evident, since the object is of scattering nature, whereas in the second case, sensitivity to $\mu_{a,2}$ is higher. This can be clearly seen from the shape of the spots (elongated in the *y*- and *x*-directions, respectively). Another interesting point is that numerical simulations that implicitly take into account all the terms in field expansion of equations (3.2)–(3.4), follow the predictions of equations (3.8) and (3.9), and equation (3.14), obtained under quasi-static assumption. This might be accepted since the objects under analysis are smaller than the wavelength of excitation but it also demonstrates the importance of the analysis carried out in this work. The parameters of the cloaking shell can be obtained using available materials [30,31], and the negative absorption coefficient of figure 3*b* can, for example, be obtained using active (emitting) media (e.g. [41,42]).

Far-field patterns of the fields scattered from (i) the bare scattering object, (ii) scattering object cloaked with the optimal parameters obtained from figure 3*a*, (iii) the bare absorbing object
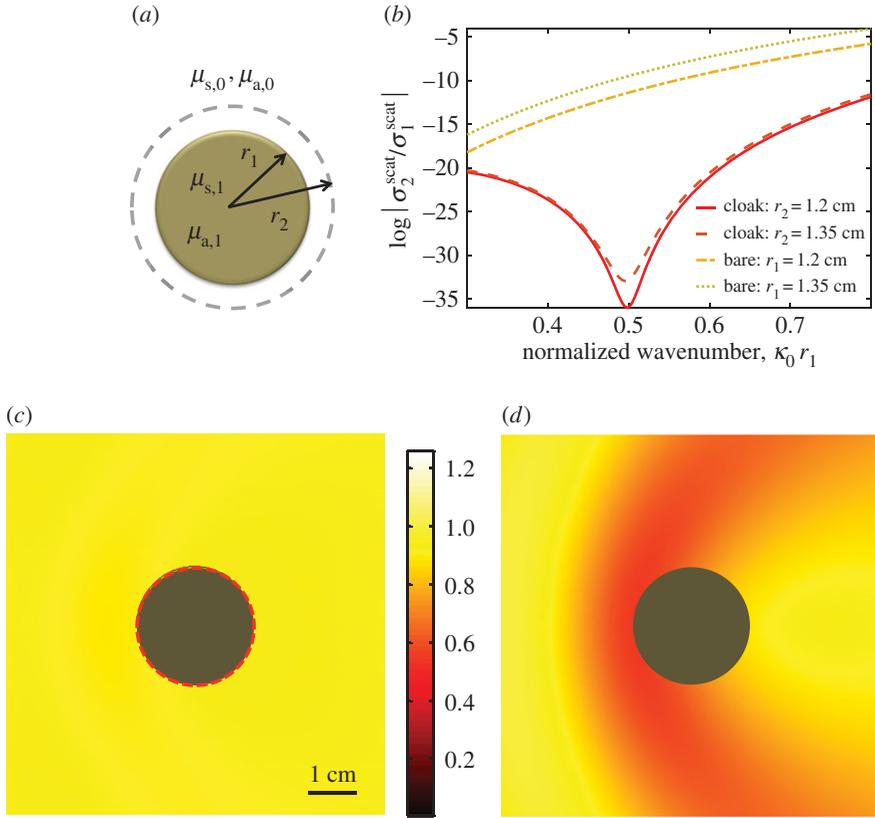
Figure 5. (*a*) Cross section of the mantle cloaking structure with the dashed grey line showing ultra-thin shell with tailored impedance. (*b*) The SCS of the total structure σ_2^{scat} normalized with the SCS of the bare object σ_1^{scat} versus normalized wavenumber $\kappa_0 r_1$, for two radii of the mantle and bare objects with the same radii, for comparison. Amplitude of DPDWs for (*c*) the mantle-cloaked object and (*d*) bare scattering object. (Online version in colour.)

and (iv) the absorbing object cloaked with the optimal parameters obtained from figure 3*b* are provided in figure 4*a–d*, respectively. These figures plot the scattering amplitude in polar coordinates, on the *x–y* plane. Significant scattering can be noticed in figure 4*a,c*, while figure 4*b,d* show that both the scattering and absorbing types of objects can be made almost undetectable at all angles, in the far-field.

(c) Mantle cloaking

Figure 5*b* plots the SCS of two mantle-cloaked objects as schematized in figure 5*a* for $r_2 = 1.2$ cm and $r_2 = 1.35$ cm. For the computation of the scattering cross section, it is assumed that the surface reactance X_d does not vary with frequency (this is a good approximation in a range of wavenumbers around $\kappa_0 r_1$). In the same figure, scattering cross section of the uncloaked objects with $r_1 = 1.2$ cm and $r_1 = 1.35$ cm are also shown for comparison. Note that $\mu_{s,1}$ and $\mu_{a,1}$ are the same as those provided in figure 3*b*. It is clear that an excellent scattering reduction is achieved over a wide range of frequencies for both cloaks. Figure 5*c,d* shows the amplitude of the scattered field in the whole computation domain for the mantle-cloaked object with $r_1 = r_2 = 1.2$ cm and the uncloaked object with $r_1 = 1.2$ cm, respectively. It is clear that when the object is cloaked, both forward and backward scatterings nearly vanish.

5. Summary

A cloaking mechanism for objects under excitation by DPDWs is studied analytically and numerically. In particular, it is shown that a cloaking shell with tailored diffusivity and photon lifetime or mantle shell with tailored impedance, drastically reduces the scattering from an enclosed spherical object. The results presented in this work help making the cloaking theory one step closer to its practical realization for diffusive light. This mechanism has potential applications in building non-invasive medical imaging devices with moderately broadband features.

References

1. Leonhardt U. 2006 Optical conformal mapping. *Science* **312**, 1777–1780. (doi:10.1126/science.1126493)
2. Pendry JB, Schurig D, Smith DR. 2006 Controlling electromagnetic fields. *Science* **312**, 1780–1782. (doi:10.1126/science.1125907)
3. Schurig D, Mock J, Justice B, Cummer SA, Pendry J, Starr A, Smith D. 2006 Metamaterial electromagnetic cloak at microwave frequencies. *Science* **314**, 977–980. (doi:10.1126/science.1133628)
4. Guenneau S, McPhedran RC, Enoch S, Movchan AB, Farhat M, Nicorovici N-AP. 2011 The colours of cloaks. *J. Opt.* **13**, 024014. (doi:10.1088/2040-8978/13/2/024014)
5. Sihvola A. 2007 Metamaterials in electromagnetics. *Metamaterials* **1**, 2–11. (doi:10.1016/j.metmat.2007.02.003)
6. Alù A, Engheta N. 2009 Cloaking a sensor. *Phys. Rev. Lett.* **102**, 233901. (doi:10.1103/PhysRevLett.102.233901)
7. Alù A, Engheta N. 2010 Cloaked near-field scanning optical microscope tip for noninvasive near-field imaging. *Phys. Rev. Lett.* **105**, 263906. (doi:10.1103/PhysRevLett.105.263906)
8. Fleury R, Monticone F, Alù A. 2015 Invisibility and cloaking: origins, present, and future perspectives. *Phys. Rev. Appl.* **4**, 037001. (doi:10.1103/PhysRevApplied.4.037001)
9. Farhat M, Chen P-Y, Guenneau S, Enoch S, McPhedran R, Rockstuhl C, Lederer F. 2011 Understanding the functionality of an array of invisibility cloaks. *Phys. Rev. B* **84**, 235105. (doi:10.1103/PhysRevB.84.235105)
10. Kerker M. 1975 Invisible bodies. *J. Opt. Soc. Am. A* **65**, 376–379. (doi:10.1364/JOSA.65.000376)
11. Chew H, Kerker M. 1976 Abnormally low electromagnetic scattering cross sections. *J. Opt. Soc. Am. A* **66**, 445–449. (doi:10.1364/JOSA.66.000445)
12. Alù A, Engheta N. 2005 Achieving transparency with plasmonic and metamaterial coatings. *Phys. Rev. E* **72**, 016623. (doi:10.1103/PhysRevE.72.016623)
13. Milton GW, Nicorovici N-AP. 2006 On the cloaking effects associated with anomalous localized resonance. *Proc. R. Soc. A* **462**, 3027–3059. (doi:10.1098/rspa.2006.1715)
14. Engheta N, Alú A. 2007 Plasmonic materials in transparency and cloaking problems: mechanism, robustness, and physical insights. *Opt. Express* **15**, 3318–3332. (doi:10.1364/OE.15.003318)
15. Rainwater D, Kerkhoff A, Melin K, Soric J, Moreno G, Alù A. 2012 Experimental verification of three-dimensional plasmonic cloaking in free-space. *New J. Phys.* **14**, 013054. (doi:10.1088/1367-2630/14/1/013054)
16. Mühlig S, Farhat M, Rockstuhl C, Lederer F. 2011 Cloaking dielectric spherical objects by a shell of metallic nanoparticles. *Phys. Rev. B* **83**, 195116. (doi:10.1103/PhysRevB.83.195116)

17. Mühlig S, Cunningham A, Dintinger J, Farhat M, Hasan SB, Scharf T, Bürgi T, Lederer F, Rockstuhl C. 2013 A self-assembled three-dimensional cloak in the visible. *Sci. Rep.* **3**, 2328. (doi:10.1038/srep02328)
18. Alù A. 2009 Mantle cloak: invisibility induced by a surface. *Phys. Rev. B* **80**, 245115. (doi:10.1103/PhysRevB.80.245115)
19. Farhat M, Rockstuhl C, Bağcı H. 2013 A 3D tunable and multi-frequency graphene plasmonic cloak. *Opt. Express* **21**, 12 592–12 603. (doi:10.1364/OE.21.012592)
20. Cai W, Chettiar UK, Kildishev AV, Shalaev VM. 2007 Optical cloaking with metamaterials. *Nat. Photonics* **1**, 224–227. (doi:10.1038/nphoton.2007.28)
21. Farhat M, Guenneau S, Movchan A, Enoch S. 2008 Achieving invisibility over a finite range of frequencies. *Opt. Express* **16**, 5656–5661. (doi:10.1364/OE.16.005656)
22. Farhat M, Guenneau S, Enoch S. 2012 Broadband cloaking of bending waves via homogenization of multiply perforated radially symmetric and isotropic thin elastic plates. *Phys. Rev. B* **85**, 020301. (doi:10.1103/PhysRevB.85.020301)
23. Chen P-Y, Farhat M, Guenneau S, Enoch S, Alù A. 2011 Acoustic scattering cancellation via ultrathin pseudo-surface. *Appl. Phys. Lett.* **99**, 191913. (doi:10.1063/1.3655141)
24. Farhat M, Chen P-Y, Guenneau S, Enoch S, Alù A. 2012 Frequency-selective surface acoustic invisibility for three-dimensional immersed objects. *Phys. Rev. B* **86**, 174303. (doi:10.1103/PhysRevB.86.174303)
25. Guild M, Haberman MR, Alù A. 2011 Plasmonic cloaking and scattering cancellation for electromagnetic and acoustic waves. *Wave Morion* **48**, 468–482. (doi:10.1016/j.wavemoti.2011.02.006)
26. Guild M, Haberman MR, Alù A. 2012 Plasmonic-type acoustic cloak made of a bilaminate shell. *Phys. Rev. B* **86**, 104302. (doi:10.1103/PhysRevB.86.104302)
27. Farhat M, Chen P-Y, Bağcı H, Enoch S, Guenneau S, Alù A. 2014 Platonic scattering cancellation for bending waves in a thin plate. *Sci. Rep.* **4**, 04644. (doi:10.1038/srep04644)
28. Farhat M, Chen P-Y, Bagci H, Amra C, Guenneau S, Alù A. 2015 Thermal invisibility based on scattering cancellation and mantle cloaking. *Sci. Rep.* **5**, 9876. (doi:10.1038/srep09876)
29. Cheong W-F, Prahl SA, Welch AJ. 1990 A review of the optical properties of biological tissues. *IEEE J. Quant. Electron.* **26**, 2166–2185. (doi:10.1109/3.64354)
30. Boas D, O'Leary M, Chance B, Yodh A. 1993 Scattering and wavelength transduction of diffuse photon density waves. *Phys. Rev. E* **47**, R2999–R3002. (doi:10.1103/PhysRevE.47.R2999)
31. O'leary M, Boas D, Chance B, Yodh A. 1992 Refraction of diffuse photon density waves. *Phys. Rev. Lett.* **69**, 2658–2661. (doi:10.1103/PhysRevLett.69.2658)
32. Schittny R, Kadic M, Bückmann T, Wegener M. 2014 Invisibility cloaking in a diffusive light scattering medium. *Science* **345**, 427–429. (doi:10.1126/science.1254524)
33. Schittny R, Niemeyer A, Kadic M, Bückmann T, Naber A, Wegener M. 2015 Diffuse-light all-solid-state invisibility cloak. *Opt. Lett.* **40**, 4202–4205. (doi:10.1364/OL.40.004202)
34. Huang D *et al.* 1991 Optical coherence tomography. *Science* **254**, 1178–1181. (doi:10.1126/science.1957169)
35. Den Outer PN, Lagendijk A, Nieuwenhuizen TM. 1993 Location of objects in multiple-scattering media. *J. Opt. Soc. Am. A* **10**, 1209–1218. (doi:10.1364/JOSAA.10.001209)
36. Kryder MH, Gage EC, McDaniel TW, Challener W, Rottmayer RE, Ju G, Hsia Y-T, Erden MF. 2008 Heat assisted magnetic recording. *Proc. IEEE* **96**, 1810–1835. (doi:10.1109/JPROC.2008.2004315)
37. Furutsu K, Yamada Y. 1994 Diffusion approximation for a dissipative random medium and the applications. *Phys. Rev. E* **50**, 3634–3640. (doi:10.1103/PhysRevE.50.3634)
38. Frank M, Klar A, Larsen E, Yasuda S. 2007 Approximate models for radiative transfer. *Bull. Inst. Math. Acad. Sinica* **2**, 409–432.
39. Heizler SI. 2010 Asymptotic telegrapher's equation (p1) approximation for the transport equation. *Nucl. Sci. Eng.* **166**, 17–35. (doi:10.13182/NSE09-77)
40. Tromberg BJ, Svaasand LO, Tsay T-T, Haskell RC. 1993 Properties of photon density waves in multiple-scattering media. *Appl. Opt.* **32**, 607–616. (doi:10.1364/AO.32.000607)
41. Seidel J, Grafstrom S, Eng L. 2005 Stimulated emission of surface plasmons at the interface between a silver film and an optically pumped dye solution. *Phys. Rev. Lett.* **94**, 177401. (doi:10.1103/PhysRevLett.94.177401)
42. Renthlei L, Wanare H, Ramakrishna SA. 2015 Enhanced propagation of photon density waves in random amplifying media. *Phys. Rev. A* **91**, 043825. (doi:10.1103/PhysRevA.91.043825)